Low atmospheric CO_2 during the Little Ice Age due to cooling-induced terrestrial uptake – Supplementary Information

Rubino, M.[1,*] Etheridge, D.M.[1] Trudinger, C.M.[1] Allison, C.E.[1] Rayner P.J.[2] Enting, I.[1,3] Mulvaney, R.[4] Steele, L.P.[1] Langenfelds, R.L.[1] Sturges, W.T. [5] Curran, M.A.J.[6,7] Smith, A.M.[8]

Affiliations: [1] CSIRO Oceans and Atmosphere, PMB 1, Aspendale, Victoria, 3195, Australia.

[2] School of Earth Sciences, University of Melbourne, 3010, Victoria, Australia

[3] ARC Centre of Excellence for Mathematics and Statistics of Complex Systems (MASCOS), University of Melbourne, 3010, Victoria, Australia

[4] British Antarctic Survey, Madingley Road, Cambridge CB3 0ET, UK

[5] Centre for Ocean and Atmospheric Sciences, School of Environmental Sciences, University of East Anglia, Norwich, Norfolk NR4 7TJ, UK

[6] Australian Antarctic Division, 203 Channel Highway, Kingston Tasmania 7050, Australia

[7] Antarctic Climate and Ecosystems Cooperative Research Centre, University of Tasmania, Hobart 7001, Australia

[8] Australian Nuclear Science and Technology Organisation (ANSTO), PMB 1, Menai, NSW 2234, Australia

[*] now at: Dipartimento di matematica e fisica, Seconda Università di Napoli, viale Lincoln 5, 81100 Caserta, Italy

Contents

1. LIA to pre-industrial COS variation

Sources (Gg of S/year)	Present	Pre-industrial	LIA
Direct COS flux from oceans	39	39	39
Indirect COS flux as DMS from oceans	81	81	81
Indirect COS flux as CS_2 from oceans	156	156	156
Direct anthropogenic flux	64	0	0
Indirect anthropogenic flux from CS_2	192	0	0
Indirect anthropogenic flux from DMS	0.5	0	0
Biomass burning	136	70	70
Photochemical ocean flux	600	600 (469)	600 (469)
Sinks (Gg of S/year)			
Destruction by OH radical	-101	-80 (-70)	-83 (-73)
Uptake by canopy	-738	-585 (-504)	-583 (-502)
Uptake by soil	-355	-281 (-242)	-279 (-241)
k_{OH}	0.21	0.21	0.21
k_{canopy}	1.52	1.52	1.45
k_{soil}	0.73	0.73	0.70
[COS] (ppt)			
measured	484	330	
calculated at balance; net total=0	514	383.5 (330)	401.6 (346)
Net total (Gg of S/year)			
with measured [COS]	74.5	132	
with calculated [COS] at balance	0	0 (0)	0 (0)

Supplementary Table 1: Global sources and sinks (in Gigagrams of Sulphur/year) of COS for the three time slices considered in this study (Present[1,2], Pre-industrial and Little Ice Age), as well as COS concentrations (in ppt) measured or calculated assuming equilibrium (net total equals zero) between sources and sinks. The sensitivity of our calculation to changes in Photochemical ocean flux is tested by setting it to 482 Gg of S/year. The corresponding sinks and COS at balance (net total=0) is shown in parenthesis.

2. Antarctic Sampling Sites

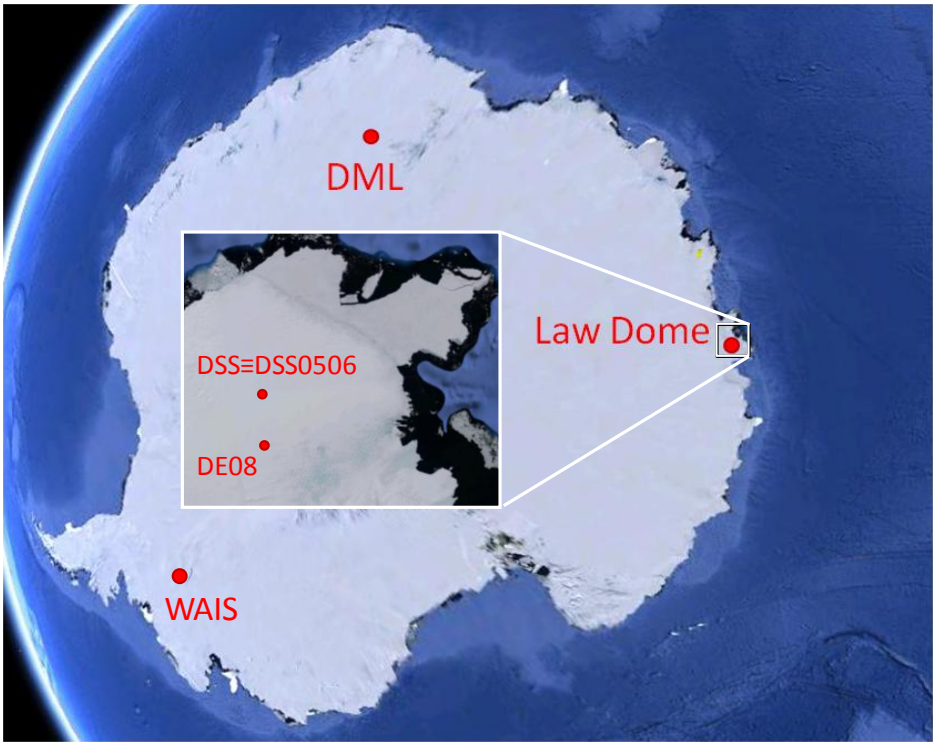

Supplementary Figure 1: Approximate location of the sampling sites

3. Ice age, gas age and gas age distribution for DML and DSS0506

3.1 DML firn air modelling

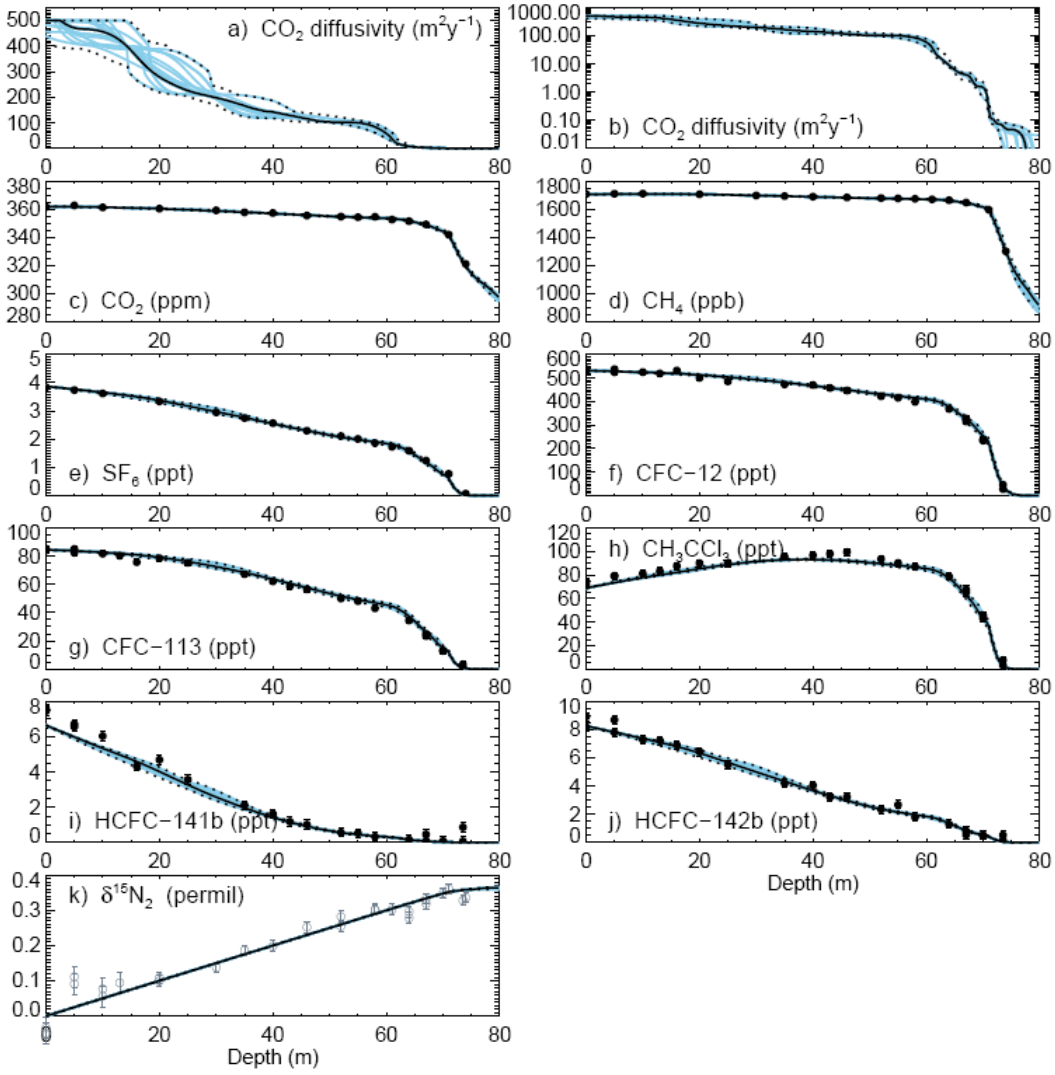

Supplementary Figure 2: a) and b): CO_2 diffusivity firn profile (linear and log y-axes); c) to k): Modelled[3] and measured[4] firn profiles for nine tracers measured in DML firn. Solid symbols indicate measurements used for optimisation of diffusivity, open symbols were not used for optimisation. The black solid line is the best case, dashed black lines show 95% confidence intervals and the blue curves show representative solutions within this confidence interval.

3.2 Gas age distribution

Gas diffusion in firn and the gradual close off of bubbles cause the air trapped in ice to have an age distribution. The width of the age distribution increases with firn depth and (for relatively stable climatic conditions) becomes constant when diffusion stops and air is completely sealed in bubbles (at the close-off depth). Because of the lower accumulation rate and temperature, the age distribution at DML is much wider than that at DSS (see Figure 2c in the main text). Consequently, DML provides a more smoothed representation of changes of atmospheric composition than DSS.

To allow consistent comparison with the DML CO_2 record, the DSS CO_2 record could be smoothed through the DML age distribution. This assumes that the CO_2 record from DSS represents the "real" atmospheric CO_2 history. This is a good first-order approximation, given how much more smoothed DML is in comparison to DSS. However, in order to perform a more accurate comparison, we have produced a synthetic CO_2 atmospheric history and then convolved this through the DML age distribution. The synthetic CO_2 atmospheric history has been generated by finding a scenario that, when smoothed through the DSS age distribution, would provide the closest (according to a chi-squared criterion) reconstruction to the DSS observation. Eighty (80) scenarios were produced by multiplying the second derivative of the spline fit to the DSS CO_2 record by an integer coefficient n ($20<n<100$), and then fitting a cubic spline to the second derivative curve. Convolving our best atmospheric CO_2 history through the DML age distribution provides the CO_2 record that would be measured in DML ice if it was consistent with the record from DSS. The DML-smoothed representation of our best atmospheric CO_2 scenario closely reproduces the 1500-1590 AD CO_2 decrease recorded in DML ice, providing evidence that the CO_2 records from DSS and DML ice are compatible (figure 2a of the main text).

The difference between the DML-smoothed representation of our best atmospheric CO_2 scenario and the DML CO_2 datapoints is comparable with the uncertainties associated with the DML CO_2 measurements. The largest discrepancies are found around 1335-1450, 1630-1670 and 1740-1770, with a maximum difference of 2.1 ppm around 1650. At present, it is unknown what causes this difference. The most likely explanation is underestimated variability associated with storage/extraction/analysis. In-situ production of CO_2 in ice due to reaction of impurities[5] is considered unlikely since the low levels of carbon monoxide (CO, see section 4.2, Supplementary Figure 3b) suggests that production of CO_2 due to reaction of organic molecules is not significant in DML ice[5,6].

We have repeated the same calculation with the WAIS CO_2 record[7]. The age distribution for WAIS has an intermediate spread between DSS and DML (see figure 2c on the main text). The WAIS CO_2 record is on average 3-6 ppm higher than the DSS CO_2 record[7]. To test whether the new DML CO_2 record is in agreement with the WAIS CO_2 trend, we have derived a CO_2 atmospheric reconstruction from the WAIS CO_2 record in the same way as for DSS, and smoothed it with the DML age distribution. This makes it possible to compare the DML-smoothed DSS-derived atmospheric reconstruction to the DML-smoothed WAIS-derived atmospheric reconstruction to see which of the two more closely reproduces the new CO_2 record from DML. The DSS derived-CO_2 reconstruction agrees with the CO_2 decrease and overall level measured in DML better than the WAIS derived-CO_2

reconstruction, suggesting that DML supports the CO_2 decrease measured at DSS as a real atmospheric feature (Figure 2a of the main text).

3.3 Corrections for Gravitational and Diffusion Fractionation

Gravitational enrichment of heavier species in air in the firn open porosity[8] causes the CO_2 concentration and $\delta^{13}C$ measured in firn and ice to be higher (more positive) than the original atmospheric values, and needs to be taken into account to correct the measured values to produce an atmospheric record. For CO_2 measurements, the correction for gravitational fractionation is calculated by multiplying the measured (or modelled when there was no measurement available) $\delta^{15}N$ of N_2 at any depth by the measured CO_2 concentration at the same depth[9]. The firn model gives $\delta^{15}N$ of 0.32 ± 0.04 ‰ and 0.272 ± 0.012 ‰ for DML and DSS0506 ice respectively, corresponding to a CO_2 correction around 1.5 ppm for DML and 1.3 ppm for DSS0506. To estimate the $\delta^{13}C$ gravitational correction to be applied, the firn model is run for ^{12}C-CO_2 and ^{13}C-CO_2 with constant CO_2 atmospheric levels[10]. The $\delta^{13}C$ gravitational correction was 0.32 ± 0.04 ‰ and 0.266 ± 0.012 ‰ for DML and DSS0506 respectively.

For measurements of isotopic ratios in firn and ice air samples, a diffusion correction is needed[10]. This correction arises from the fact that an isotope ratio is the ratio of two isotopes with slightly different diffusion coefficients and therefore slightly different effective ages. For hypothetical species with constant isotopic ratio, but changing atmospheric concentrations, the isotopic ratio in the firn can be significantly different than the atmospheric ratio. For $\delta^{13}C$, the diffusion correction is proportional to the rate of change of CO_2 concentration. The diffusion correction ranged between -0.026 and 0.046 ‰, and -0.003 and 0.062 ‰ for DML and DSS0506 respectively, with uncertainty lower than 0.01 ‰.

4 Reliability of the CO_2 and $\delta^{13}C$-CO_2 records: independent evidence

4.1 Overlap between DML, DSS0506 and DE08

The consistency between ice core, firn and direct atmospheric measurements of CO_2 and $\delta^{13}C$ provides evidence that we can reliably extend the atmospheric CO_2 and $\delta^{13}C$ records back in time. Figure 1 of the main text has shown that CO_2 measurements from DML are compatible with those from DSS when the different gas age distributions are taken into account. The overlap between CO_2 and $\delta^{13}C$ measurements from Law Dome ice (DSS, DE08 and DE08-2), different firn sites (South Pole, DSSW20K, DE08-2) and the Cape Grim station has been already demonstrated[11]. Supplementary Figure 3a shows that the $\delta^{13}C$ measurements from DML (red symbols in Supplementary Figure 3a) and DSS0506 (blue symbols in Supplementary Figure 3a) overlap the DE08 measurements previously published[11] (2013, yellow symbols in Supplementary Figure 3a).

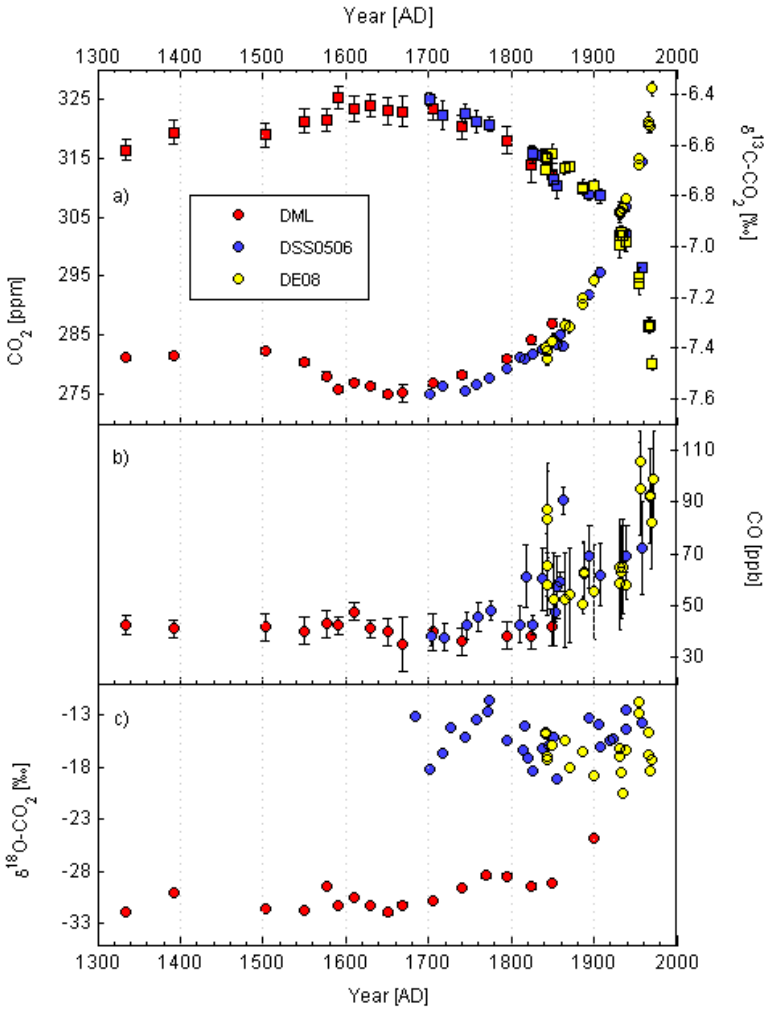

Supplementary Figure 3: Measurements of a) $\delta^{13}C$-CO_2, CO_2, b) CO and c) $\delta^{18}O$-CO_2 from DML (red), DSS0506 (blue) and DE08 (yellow)

4.2 Analyses of Carbon monoxide (CO)

Measurements of CO can provide evidence of sample contamination. This could occur in the ice sheet (in-situ) through reactions of organic molecules in the ice[5,6], or during the storage-extraction-analysis procedure of the ice samples[11]. Being a product of oxidation, if the CO concentration is altered (typically higher than the expected one), the original CO_2 concentration (and consequently its $\delta^{13}C\text{-}CO_2$) is likely to be altered too. The CO concentration measured in DML ice (Supplementary Figure 3b) is consistent with previously published measurements over the last 650 years[12], supporting the reliability of the DML CO_2 and $\delta^{13}C\text{-}CO_2$ record. For DSS0506 and DE08, CO measurements are generally higher than for DML. The sites of DSS0506 and DE08 are warmer than that of DML and chemical reactions are more likely to occur in DSS0506 and DE08 ice. Therefore, we attribute this difference to in-situ production of CO. CO is thought to be produced in warm ice due to the reaction between hydroxyl radicals and peroxides with organic molecules, or the photochemical degradation of dissolved organic matter[13]. However, all samples used here have sufficiently low CO[11] to ensure reliable CO_2 and $^{13}CO_2$. This is especially true for DML ice, where very low CO values provide evidence that records of gases from DML ice are unlikely to be altered by production occurring in-situ or during the storage-extraction-analysis procedure.

4.3 Analyses of $\delta^{18}O\text{-}CO_2$

The $\delta^{18}O\text{-}CO_2$ is measured together with the $\delta^{13}C\text{-}CO_2$ in a typical dual inlet IRMS acquisition. In firn air, the $\delta^{18}O$ has been shown[14] to be shifted away from atmospheric values toward isotope equilibrium with H_2O from precipitation ($\delta^{18}O\text{-}H_2O_{ICE}$). Here we show that the $\delta^{18}O$ measured in DML, DSS0506 and DE08 ice is consistent with that view. Supplementary Figure 3 shows that DML $\delta^{18}O$ measurements decrease continuously going back in time, from -25 ‰ to -32 ‰, while $\delta^{18}O$ measurements from DSS0506 and DE08 are scattered around -15 ‰. Compared to DSS0506 and DE08, DML ice comes from higher latitude, thus showing more ^{18}O-depleted values, according to the $\delta^{18}O\text{-}H_2O_{ICE}$ that follows the meteoric water line[15]. Additionally, as DML is characterised by low accumulation rate (see section SI2 and Figure 1c of the main text), each air sample extracted from a 1 kg of DML ice has been in contact with ice with a large distribution of ages during the period between bubble close off and sampling (at least a century). The $\delta^{18}O$ measured in each DML ice sample is, therefore, the average of the $\delta^{18}O$ that each parcel of air gets from the surrounding ice ($\delta^{18}O\text{-}H_2O_{ICE}$) while exchanging O-isotopes. DSS0506 and DE08 have higher accumulation than DML and each gas sample we analysed had been in contact with ice characterised by an age distribution of less than a year. Thus, the $\delta^{18}O\text{-}CO_2$ in DSS0506 and DE08 ice comes from the isotopic equilibrium between the initial $\delta^{18}O\text{-}CO_2$ and the surrounding $\delta^{18}O\text{-}H_2O_{ICE}$ of a specific season. The seasonal fluctuation of the $\delta^{18}O\text{-}H_2O_{ICE}$ signal explains the variation of the $\delta^{18}O\text{-}CO_2$ in DSS0506 and DE08 ice. Measurements of $\delta^{13}C\text{-}CO_2$ are influenced by any non mass dependent alteration of the $\delta^{18}O\text{-}CO_2$, given that it is obtained after a correction based on the measured $\delta^{45}CO_2$ and $\delta^{46}CO_2$ and the assumed distribution of O-isotopes (the so-called ^{17}O correction[16]). Therefore, the consistency

between our $\delta^{18}O$-CO_2 results and accepted interpretation[14] adds extra value to the reliability of our new DML, DSS0506 and DE08 $\delta^{13}C$-CO_2 records.

5. Sample selection

Sample selection is performed according to several criteria[11] including consideration of the quality of:

1. The ice samples;
2. The extraction procedure;
3. The analysis protocol.

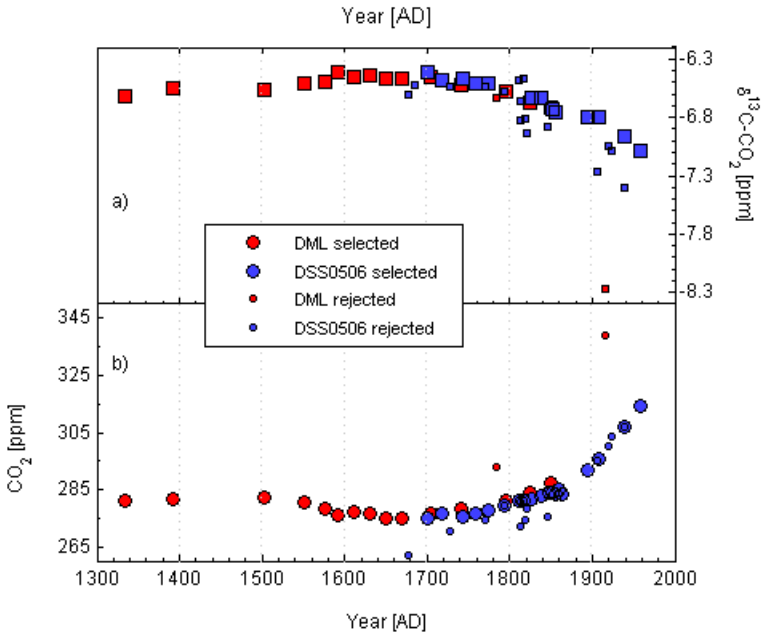

Supplementary Figure 4: selected (large circles and squares) and rejected (small circles and squares) CO_2 and $\delta^{13}C$-CO_2 from DML (red) and DSS0506 (blue)

A total of 18 measured samples were rejected (small symbols in Supplementary Figure 4) because they do not pass the selection thresholds chosen to get a high precision record. Of the 18, just two are from DML, the rest from DSS0506. For DML, the samples are rejected because of an unrealistically high concentration of CO (>30 ppb higher than the neighbouring CO concentrations for that age) and CO_2 (>5 ppm higher than the neighbouring/well established CO_2 concentrations for that age). Correspondingly, a very low $\delta^{13}C$ is measured, suggesting that those two samples are contaminated with modern air.

For DSS0506, 10 samples are rejected because of difficulties during the analysis by IRMS (when a sample stays in the sample volume for over 12 hours before analysis and when one or more standards in a sequence run are rejected indicating that lower precision and accuracy than usual can be achieved). The other 6 rejected samples are discarded because an unrealistically low CO_2 concentration is measured (>5 ppm lower than the neighbouring/well established CO_2

concentrations for that age). In our experience, CO_2 and N_2O concentrations can be lowered in ice that has been exposed to post-coring melting (CO_2 and N_2O being the most soluble among the gases we measure). However, 4 of the 6 rejected samples provide enough air to measure N_2O, which does not show any major difference (not shown) compared to the N_2O measured in coeval samples from other cores[17]. We don't have a definite explanation for the low CO_2 measured in DSS0506. However, we have recently measured a decline in the CO_2 concentration of some DSS samples compared to immediately adjacent samples in the same core measured previously[17,18]. Since the two cores (DSS0506 and DSS) were stored in the same freezer in Hobart (Tasmania, Australia), we interpret the low CO_2 as a recent effect of storage.

None of the ice cores in this study reached depths or temperatures sufficient for clathrate formation which can affect the extraction and measurement of enclosed gases and ^{13}C-CO_2 in particular[19].

6. Carbon cycle sensitivity to temperature

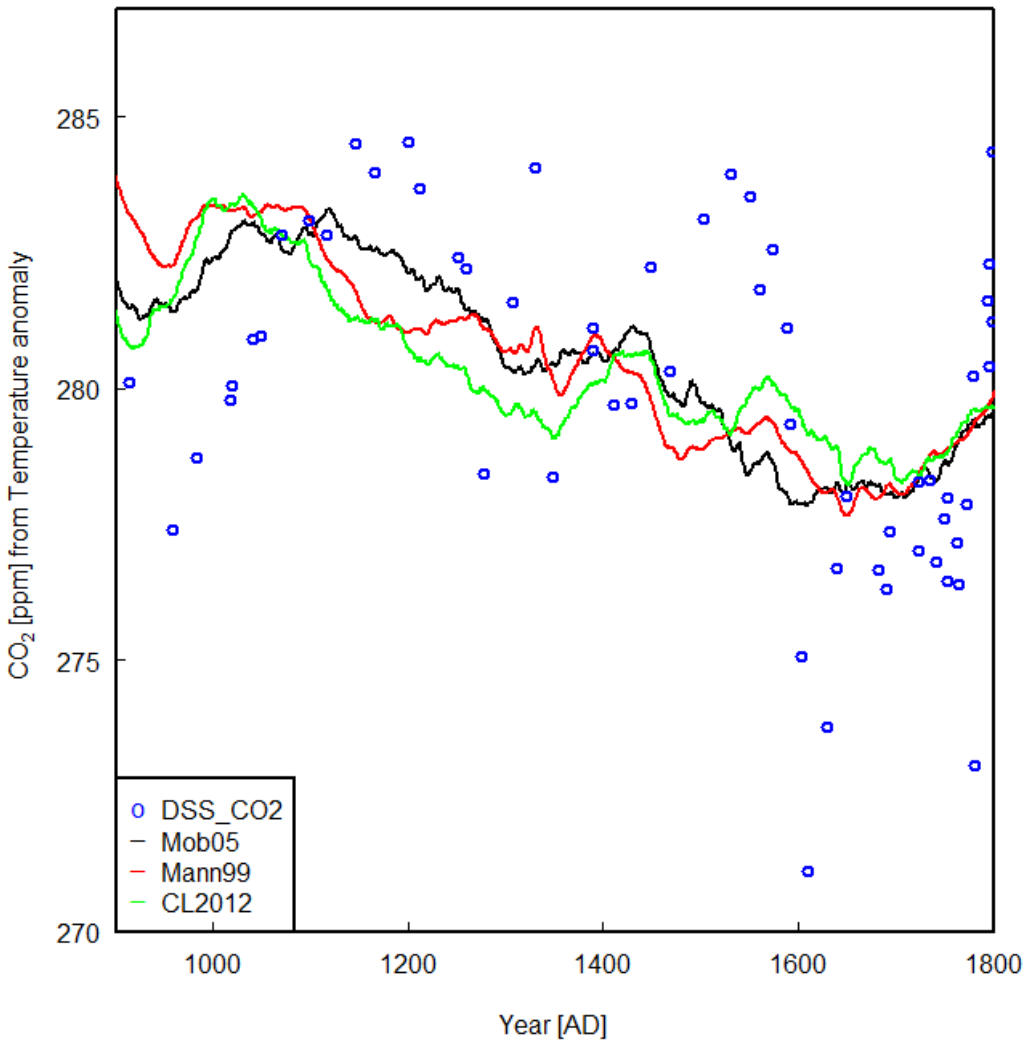

Supplementary Figure 5: DSS CO_2 record (blue circles) and CO_2 concentration (lines) obtained by multiplying different temperature reconstructions (black: Moberg et al. (2005)[20], red: Mann et al., (2009)[21], green: Christiansen and Ljungqvist (2012)[22]) by $\gamma_X^{'}$ that minimises the difference in equation (SE8) within the fitting interval 1000-1750 AD.

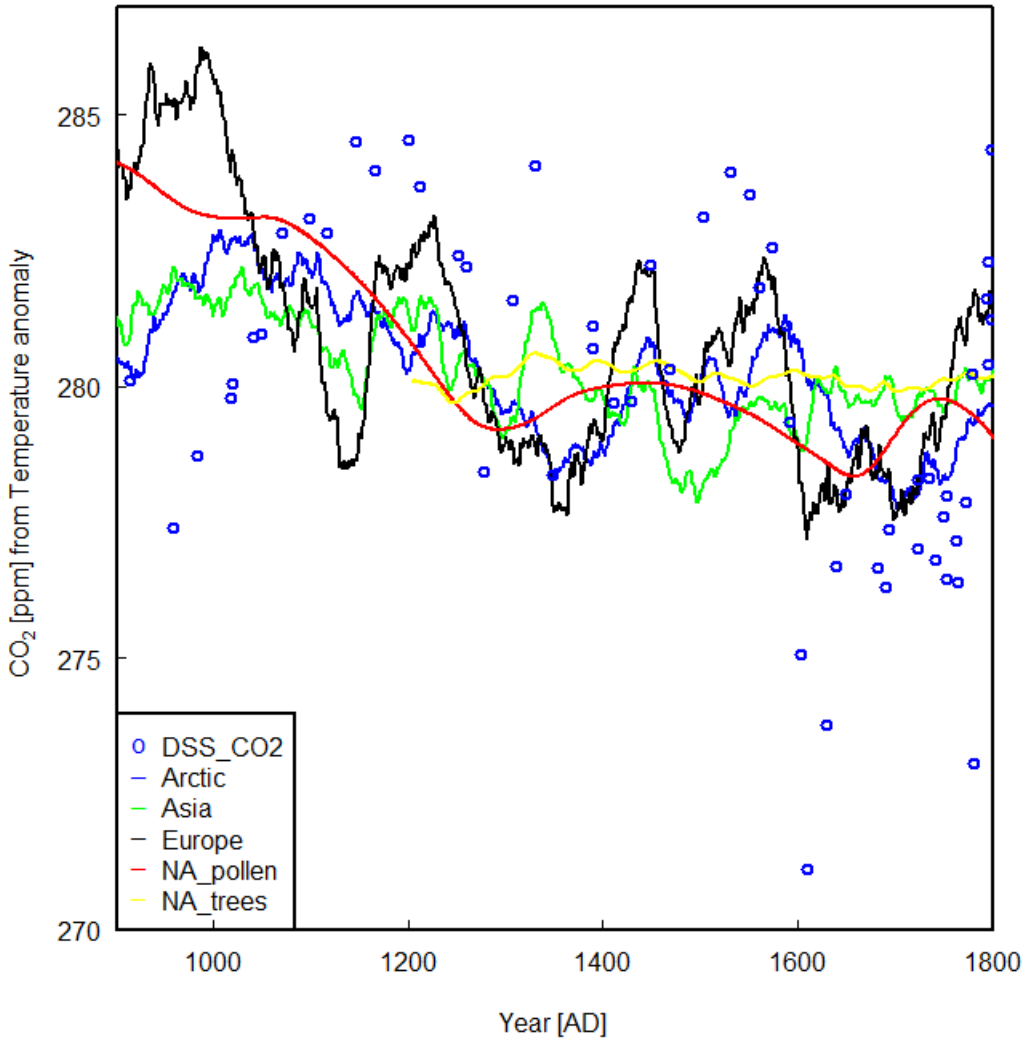

Supplementary Figure 6: DSS CO_2 record (blue circles) and CO_2 concentration (lines) obtained by multiplying the Northern Hemisphere PAGES[23] temperature reconstructions (blue: Arctic, black: Europe, green: Asia, red: North American pollen, yellow: North America trees) by γ_X' that minimises the difference in equation (SE8) within the fitting interval 1000-1750 AD.

	Region	500-1750	1000-1750	1300-1750	1500-1800
n		59	43	29	32
Mob05	NH	0.434	0.488	0.734	1.349
Mann99	NH	0.147	0.636	1.161	2.200
CL2012	>30N	0.159	0.200	0.482	0.638
PAGES	Arctic	0.319	0.437	0.414	0.538
PAGES	Asia	0.256	0.526	-0.012	-0.219
PAGES	Europe	0.282	0.837	1.328	1.180
PAGES	NA_pollen	0.489	0.898	2.813	1.638
PAGES	NA_trees	0.198	0.119	0.645	-0.004

Supplementary Table 2: Estimates of $\gamma_X^{'}$ (in PgC yr^{-1} K^{-1}) obtained by regression of DSS concentrations against temperature records convolved with the CO_2 response function (R(t)), and an exponential source response (H(t)), for various time intervals (shown in top line) and various temperature reconstructions (X). The number of DSS data points in each interval is n. The temperature reconstructions are: M2005[20] (Moberg et al., 2005); Mann99[21] (Mann et al., 1999); CL2012[22] (Christiansen and Ljungqvist, 2012), PAGES[23] (Pages2k, 2013).

References

1. Berry, J. et al. A coupled model of the global cycles of carbonyl sulfide and CO_2: A possible new window on the carbon cycle. *J. Geophys. Res-Biogeo.* **118,** 842-852 (2013)

2. Campbell, J.E. et al. Atmospheric carbonyl sulfide sources from anthropogenic activity: Implications for carbon cycle constraints. *Geophys. Res. Lett.* **42**, 8: 3004-3010 (2015)

3. Trudinger, C.M. et al. How well do different tracers constrain the firn diffusivity profile? *Atmos. Chem. Phys.* **13**, 1485-1510 (2013)

4. Bräunlich, M. et al. Changes in the global atmospheric methane budget over the last decades inferred from ^{13}C and D isotopic analysis of Antarctic firn air. *J. Geophys. Res.* **106**, 20456-20481 (2001)

5. Francey, R. et al., The pre-industrial difference in CO_2 from Antarctica and Greenland ice. *Extended abstract of the Fifth International Carbon Dioxide Conference.* 211-212 (1997)

6. Jenk, T. et al., Sources of excess CO_2 in Greenland ice cores. *AGU Fall Meeting.* 2012AGUFM.C54B..03J (2012)

7. Ahn, J. et al. Atmospheric CO_2 over the last 1000 years: A high-resolution record from the West Antarctic Ice Sheet (WAIS) Divide ice core. *Global. Biogeochem. Cy.* **26,** GB2027 (2012)

8. Schwander, J. Stauffer, B. Sigg, A. Air mixing in firn and the age of the air at pore close-off. *Ann. Glaciol.* **10,** 141-145 (1988)

9. Sowers, T.M. Bender, M. Raynaud, D. Elemental and isotopic composition of occluded O_2 and N_2 in polar ice. *J. Gephys. Res.* **94,** 5137-5150 (1989)

10. Trudinger, C.M. et al. Modeling air movement and bubble trapping in firn. *J. Geophys. Res.* **102**, 6747-6763 (1997)

11. Rubino, M. et al. A revised 1000 year atmospheric $\delta^{13}C$-CO_2 record from Law Dome and South Pole, Antarctica. *J. Geophys. Res-Atmos.* **118,** 8482-8499 (2013)

12. Wang, Z. Chappellaz, J. Park, K. Mak, J. E. Large variations in Southern Hemisphere biomass burning during the last 650 years. *Science.* **330,** 1663-1666 (2010)

13. Haan, D. & Raynaud, D. Ice core record of CO variations during the last two millennia: Atmospheric implications and chemical interactions within the Greenland ice. *Tellus B.* **50,** 253-262 (1998)

14. Assonov, S.S. Brenninkmeijer, C. A. M. & Jöckel, P. The ^{18}O isotope exchange rate between firn air CO_2 and the firn matrix at three Antarctic sites. *J. Gephys. Res.* **110,** D18310 (2005)

15. Craig, H. Isotopic Variations in Meteoric Waters. *Science.* **133,** 1702-1703 (1961)

16. Brand, W.A. Assonov, S. S. Coplen, T. B. Correction for the ^{17}O interference in $\delta(^{13}C)$ measurements when analyzing CO_2 with stable isotope mass spectrometry (IUPAC Technical Report). *Pure Appl. Chem.* **82,** 1719-1733 (2010)

17. MacFarling-Meure, C. et al. Law Dome CO_2, CH_4 and N_2O ice core records extended to 2000 years BP. *Geophys. Res. Lett.* **33,** L14810 (2006)

18. Etheridge, D.M. et al. Natural and anthropogenic changes in atmospheric CO_2 over the last 1000 years from air in Antarctic ice and firn. *J. Geophys. Res.* **101,** 4115-4128 (1996)

19. Schaefer, H. et al. On the suitability of partially clathrated ice for analysis of concentration and $\delta^{13}C$ of palaeo-atmospheric CO_2. *Earth Planet Sc Lett.* **307,** 334-340 (2011)

20. Moberg, A. Sonechkin, D. M. Holmgren, K. Datsenko, N. M. & Karlén, W. Highly variable Northern Hemisphere temperatures reconstructed from low- and high-resolution proxy data. *Nature* **433**, 613-617 (2005)

21. Mann, M.E. et al. Global Signatures and Dynamical Origins of the Little Ice Age and Medieval Climate Anomaly. *Science* **326**, 1256 (2009)

22 Christiansen, B. & Ljungqvist F.C. The extra-tropical Northern Hemisphere temperature in the last two millennia: reconstructions of low-frequency variability. *Clim. Past* **8**, 765-786 (2012)

23. PAGES 2k network. Continental-scale temperature variability during the past two millennia. *Nature Geosci.* **6,** 339-346 (2013)